Chemistry: Faculty Publications and Other Works

Faculty Publications and Other Works by Department

9-30-2014

Molecular Interactions with Ice: Molecular Embedding, Adsorption, Detection, and Release

K D. Gibson
University of Chicago

Grant G. Langlois
University of Chicago

Wenxin Li
University of Chicago

Daniel Killelea
dkillelea@luc.edu

S J. Sibener
University of Chicago

Follow this and additional works at: https://ecommons.luc.edu/chemistry_facpubs

Part of the Atomic, Molecular and Optical Physics Commons, and the Physical Chemistry Commons

Recommended Citation

K. D. Gibson, Grant G. Langlois, Wenxin Li, Daniel R. Killelea, and S. J. Sibener

Molecular interactions with ice: Molecular embedding, adsorption, detection, and release

K. D. Gibson,[1] Grant G. Langlois,[1] Wenxin Li,[1] Daniel R. Killelea,[2] and S. J. Sibener[1,a)]

[1]*The James Franck Institute and Department of Chemistry, The University of Chicago, 929 E. 57th Street, Chicago, Illinois 60637, USA*
[2]*Department of Chemistry and Biochemistry, Loyola University Chicago, 1068 W. Sheridan Ave., Chicago, Illinois 60660, USA*

The interaction of atomic and molecular species with water and ice is of fundamental importance for chemistry. In a previous series of publications, we demonstrated that translational energy activates the embedding of Xe and Kr atoms in the near surface region of ice surfaces. In this paper, we show that inert molecular species may be absorbed in a similar fashion. We also revisit Xe embedding, and further probe the nature of the absorption into the selvedge. CF_4 molecules with high translational energies (≥ 3 eV) were observed to embed in amorphous solid water. Just as with Xe, the initial adsorption rate is strongly activated by translational energy, but the CF_4 embedding probability is much less than for Xe. In addition, a larger molecule, SF_6, did not embed at the same translational energies that both CF_4 and Xe embedded. The embedding rate for a given energy thus goes in the order Xe > CF_4 > SF_6. We do not have as much data for Kr, but it appears to have a rate that is between that of Xe and CF_4. Tentatively, this order suggests that for Xe and CF_4, which have similar van der Waals radii, the momentum is the key factor in determining whether the incident atom or molecule can penetrate deeply enough below the surface to embed. The more massive SF_6 molecule also has a larger van der Waals radius, which appears to prevent it from stably embedding in the selvedge. We also determined that the maximum depth of embedding is less than the equivalent of four layers of hexagonal ice, while some of the atoms just below the ice surface can escape before ice desorption begins. These results show that energetic ballistic embedding in ice is a general phenomenon, and represents a significant new channel by which incident species can be trapped under conditions where they would otherwise not be bound stably as surface adsorbates. These findings have implications for many fields including environmental science, trace gas collection and release, and the chemical composition of astrophysical icy bodies in space. © *2014 AIP Publishing LLC.* [http://dx.doi.org/10.1063/1.4895970]

I. INTRODUCTION

Ice surfaces are nearly ubiquitous in nature, and collisions of gas-phase species with ice surfaces alter the composition and morphology of the ice.[1–3] In interstellar space, icy surfaces are bombarded by ions, which can penetrate well below the surface. These collisions deliver both energy and other species (C, S, N) leading to the chemical modification of the interior of the ice.[4–7] Energetic collisions of small molecules with ice surfaces are of particular relevance for the capture and matrix preconcentration of trace gases;[8,9] for gases with insufficient momentum are unable to penetrate into the ice, whereas heavier, or more energetic, species will be trapped in the near surface region of the solid.[10] Energetic collisions on ice surfaces are also highly relevant for the evolution of the composition of icy bodies in space.[11–13] In particular, collisions with impact energy of several electron volts are representative of the encounters between the surfaces of comets and the ambient molecules and atoms in interplanetary space as a comet orbits a star. The embedding of the gaseous species

in the ice surface implies that the changes in the composition of comets can be modified by other mechanisms besides thermal desorption or accretion.[1,14,15] Finally, an improved understanding of how small molecules and atoms penetrate ice surfaces and stably embed is of high importance to the formation or destruction of clathrates or other systems of trapped gases in icy matrices. Methane clathrates have received consideration as an energy source,[16] and the importance of a firm fundamental understanding of clathrates and the interactions between gases and ice was evident in the efforts in capping the oil well during the Deepwater Horizon disaster.[16–18] Another area of significance is the role of trapped methane in the permafrost in the positive feedback loop of global warming.[19–21] Finally, collisions between icy particles and gases have significance in atmospheric processes.[22,23] Because of the widespread interest in the interactions of gas phase species with ice surfaces, we have chosen to expand on our previous work with noble gas embedding on ice and now examine how small molecules can become implanted in the selvedge of ice surfaces and further study the nature of the absorption sites.

In previous papers, we explored the sputtering of ice with high translational energy Xe[2] and the scattering of fast

a)Author to whom correspondence should be addressed. Electronic mail: s-sibener@uchicago.edu

neutral Xe and Kr from the surface of ice.[10,24] On both amorphous solid water (ASW) and crystalline ice (CI), the energetic incident Xe atoms sputtered water molecules from the surface, and a well-defined, water isotope-dependent, threshold energy was observed for the sputtering that was on the order of the sublimation energy. The scattering experiments and chemical dynamics simulations[10,24] showed that the ice surfaces very efficiently accommodate the incident kinetic energy of the Xe or Kr atoms, and the energy of the scattered atoms is weakly correlated to their incident energy. These findings suggested that the scattering was not the result of simple binary collisions. Computational simulations[24] showed that the efficient energy accommodation is the result of extensive penetration of the ice by the energetic projectiles. In the course of these experiments, we discovered that a small, but significant, amount of the inert gases could be absorbed at surface temperatures well above where they could stably adsorb.[3,10] Ice was grown on single crystal metal surfaces, either Rh(111) or Au(111), in ultra-high vacuum (UHV) and were then exposed to beams of energetic Xe or Kr atoms. After the exposure, temperature programmed desorption (TPD) measurements were taken of the ice, and the signal from D_2O and either Xe or Kr was monitored as the ice temperature was ramped upwards. An exciting discovery was that Xe and Kr were observed to desorb at temperatures significantly (>50 K) above their surface desorption temperature.[25] The implication was that Xe or Kr atoms were embedded within the ice. Only when the ice was warmed during the TPD measurement could the trapped gases escape. For both Xe and Kr, the rate of implantation was directly related to the translational energy, and for a given energy, Xe embedded at a higher rate than the lighter Kr.[10,24] The amount embedded appeared to asymptotically approach a final value that was dependent on energy and mass.

These experiments also demonstrated very different embedding behaviors for CI and ASW. The morphology of the ice was determined by the deposition temperature for the ice from gas-phase water.[26–28] At temperatures below ∼135 K, ASW is formed, whereas at 140 K and above, CI forms. ASW is metastable with respect to CI, and undergoes an irreversible transition to CI at ∼160 K. On CI, Xe embedding appeared to be less probable, and the trapped gas only desorbed at a low temperature (∼140 K), before any appreciable water desorption, whereas embedded rare gas in ASW desorbed during the thermal ramp up to ∼160 K.

The focus of this paper is to more fully explore the nature of the embedding process. One question from the previous work was whether there was a difference in the adsorption sites that lead to both high and low temperature desorption, particularly since the rare gas begins to escape at an appreciable rate before the water begins desorbing. Also, we wanted to more thoroughly explore the embedding rate as a function of projectile mass and energy. In this context, we also used two other relatively inert gases with very different masses, SF_6 and CF_4. CF_4 has a strong IR signal, which allows for the use of time-resolved Fourier-transform reflection-absorption infrared spectroscopy (RAIRS) in addition to TPD. TPD is a destructive technique where constructing an uptake curve requires that each measured point be taken on a new ASW or CI

film, so the experiment becomes prohibitively time consuming using this approach alone. RAIRS allows the same measurements to be made sequentially on the same ice sample, greatly facilitating these measurements, especially for systems or conditions with low embedding rates.

Both Xe and CF_4 show low temperature (before water begins desorbing) and higher temperature features in the TPD spectra from the exposure of ASW, though the low temperature feature is much larger for Xe.[3] The uptake rate for CF_4 is much less than for Xe at the same incident energy, which is consistent with our previous observations that mass (and thus the momentum) is an important consideration. However, it also appears that the uptake rate is also less than for Kr, which has almost the same mass as CF_4. The previous experiments[10] with Xe and Kr showed that the rate of embedding decreased with exposure. The rates of CF_4 embedding vs. exposure curves were linear for all of the energies and exposures used, but the amount of CF_4 embedded had not reached a value as large as for the longest exposures of the rare gases.

By varying the TPD techniques used, we have come to the conclusion that the lower temperature TPD feature for ASW is due to adsorption just below the surface. The rest of the absorbed species escape concurrently with desorbing water, and are more deeply buried, to within ∼3–4 layers of ice below the surface. For CI, only high energy Xe is embedded, and then, only in the topmost portion of the ice; the desorption peak due to more deeply buried atoms is not observed. Even at the highest energies (∼5.3 eV), there was apparently no CF_4 embedding, even with the more sensitive RAIRS technique. Only at an energy <2.5 eV does Xe show embedding in ASW but not CI.

We also investigated whether a much larger, yet still inert, molecule could be stably embedded in ASW. We exposed ASW to a beam of SF_6 molecules (MW = 146 g mol^{-1}), but it showed no detectable embedding in ASW, even with an energy of 3 eV, the energy at which Kr, Xe, and CF_4 all show detectable embedding. Tentatively, we ascribe this to the larger radius of this molecule relative to both CF_4 and the rare gases.

In the present paper, we expand significantly on our previous results; we explore the implantation of molecular species and further probe the nature of the absorption sites for Xe by "capping" the surface of ASW after exposure to the Xe beam. Taken together, these results probe the complex interaction of energetic gas-phase species with ice, and provide further details of this exciting phenomenon. We explain our new results in the context of our previous experimental and computational findings, and improve our understanding of how the various parameters, including ice morphology, incident energy and angle, and the mass of the projectile are interrelated, leading to the penetration and stable embedding of gaseous species in ice.

II. EXPERIMENTAL

A. Thermal desorption

Experiments entailed dosing a cryogenically cooled Rh(111) target crystal with a D_2O molecular beam, then

exposing the surface to atomic beams of Xe or molecular beams of CF_4. After exposure, any absorbed gases, as well as the D_2O, were measured by performing mass spectrometric TPD experiments. The machine consists of a diffusion pumped source region, where the atomic or molecular beams were produced. The beam was skimmed, and then passed through three differential pumping regions before entering the UHV chamber and impinging upon the Rh(111) target crystal. Detection of the desorbed gases was done with a double-differential pumped quadrupole mass spectrometer, using an electron bombardment ionizer.

D_2O (m/e = 20) (Aldrich, 99.9 at. % D) was used since it had a much lower background signal than H_2O (m/e = 18) in our mass spectrometer system. This beam was produced by passing low pressure (2.25 psi (absolute)) He through a liquid filled room temperature bubbler and expanding through a 200 μm pinhole. The coverage was determined from the integrated TPD spectra, and was calibrated by comparing with the TPD signal from a monolayer (ML) grown on clean Rh(111) (1 ML = 1.07×10^{15} molecules cm^{-2}).[29] Dosing rates were estimated to be $\sim$0.5 ML s^{-1} at normal incidence. All of the dosing was done at an incident angle of $\theta = 45°$, and the total coverage was $\sim$750 ML. We explored the effect of ice thickness by performing embedding measurements on thinner ice, and found that when using CF_4 ($\langle E \rangle$ between 3 and 4.4 eV) and the Rh(111) substrate, $\sim$130 ML D_2O films had 1.5-2 times as much CF_4 as the 750 ML films. Even at 375 ML, there was possibly a slight difference in the shape of the TPD spectra. Thicker ice gave the same result as for 750 ML, which determined the thickness used in these experiments. These observations go to the self-similar structure of thick versus thin films of ice. Two forms of solid water were grown, CI at a surface temperature of 140 K and ASW at $T_S = 120$ K. At these growth conditions, the ice is not porous.[30–32]

High translational energy beams of CF_4 (Aldrich, 99.9%), SF_6 (Aldrich, > 99.75%), Xe (Airgas, 99.995%), or Kr (Praxair, Research Grade) were made by mixing <0.5% (by volume) of the gas with either H_2 or He. The mixture was expanded through a 10 or 15 μm pinhole with several hundred psi of backing pressure. The nozzle temperature could be varied between 300 and 673 K. This resulted in energies as high as $\sim$7 eV for Xe and slightly more than 5 eV for CF_4, with a $\Delta E/E \approx 0.16$. Energies were determined by measuring the time-of-flight of the incident atomic or molecular beams. This was accomplished by lowering the target and rotating the detector until it was directly in line with the beam. A rotating, slotted chopper wheel in the second differential pumping region modulated the beam, and the time for the gas to travel the distance to the detector was determined.

To estimate the flux, the first step was to use a neat beam of either CF_4 or Xe and measure the pressure rise in the UHV chamber with a nude Bayard-Alpert gauge calibrated for N_2. When corrected for the relative sensitivities, 2.31 for CF_4[33] or 2.8 for Xe,[34,35] and knowing the pumping speed, the number/sec of atoms or molecules entering the chamber could be determined. This measurement was used to calibrate a residual gas analyzer (RGA) that was not in the direct line of sight of the beam. With this calibration, and the size of the beam spot at the target crystal, it was possible to deter-

mine the flux for any of the seeded beams by using the RGA signal.

The substrate for the solid D_2O growth was a Rh(111) crystal that could be cryogenically cooled with either liquid N_2 or He, and resistively heated. This crystal was mounted on a rotatable manipulator so that the incident angle that the beam impinged on the surface could be varied. In the past, we would chemisorb a half monolayer of oxygen on the clean crystal and use this as the substrate.[10] For the experiments presented in the present paper, we determined that just flashing the crystal to $\sim$ 350 K before the ice growth gave essentially the same results, and therefore the pre-deposition O_2 exposure is unnecessary and was omitted for the results presented here. Temperature (T_S) was measured with a chromel-alumel thermocouple welded to the Rh crystal. The readings are within 2 K, verified by checking the TPD results against the kinetic parameters of Smith *et al.*[28] For all of the high translational energy gas exposures, the ice was held at 120 K. TPD spectra were taken with the detector normal to the surface and with a temperature ramp rate of 10 K min^{-1}. The detector had an electron multiplier operated in pulse counting mode. The signal was collected by a counter in 1 s bins. The m/e that the quadrupole passed was set by the voltage from a computer-controlled digital-to-analog converter. By changing the voltage at the end of each bin, it was possible to collect the results for different masses in consecutive bins. For all of the TPD spectra shown, there was signal collected for the mass of the embedded species (Xe or CF_4), as well as for the desorbing D_2O. For the Xe, the results are given in ML, where 1 ML = 6×10^{14} atoms cm^{-2}. This was calibrated by growing a single monolayer of Xe, and measuring the integrated TPD signal.[10] The sensitivity of the detector for CF_4 relative to Xe was determined from the flux measurements by comparing the signal from the straight through beam into the mass spectrometer with the RGA signal. For comparing with the Xe, the CF_4 results are also given in units of ML, with 1 ML = 6×10^{14} CF_4 molecules cm^{-2}.

B. RAIRS

Complementary sets of experiments on CF_4 embedding were performed in a separate molecular beam scattering instrument capable of monitoring changes in ice films with *in situ* RAIRS. The instrument has been described at length in previous publications.[2,36] Modifications relevant to these experiments are included herein.

Ice films were grown on a Au(111) single crystal housed inside the UHV chamber ($< 1 \times 10^{-9}$ Torr), secured to a temperature-controlled sample plate on the instrument's manipulator. All embedding experiments within the RAIRS instrument, unless elsewhere noted, were performed with the crystal held at 125 K as measured by a chromel-alumel thermocouple secured to the sample plate directly beside the crystal. The sample temperature was controlled with a combination of liquid nitrogen cooling and resistive heating of a filament located directly behind the sample. ASW ranging in thicknesses from 60 to 200 layers were grown on the crystal at 125 K by backfilling the chamber with D_2O vapor through

a leak valve to a pressure of $\sim 1 \times 10^{-7}$ Torr ($\sim$0.1 layers of D_2O s^{-1}).[27,30]

RAIRS was performed with *p*-polarized light from a commercial IR spectrometer (Nicolet 6700) directed onto the surface at 75° incidence, collected with a liquid nitrogen cooled MCT/A detector. All spectra were averages of 200 scans taken at 4 cm^{-1} resolution in reference to either the bare or ice-covered Au(111) crystal, with peaks fit to Gaussian line shapes atop cubic polynomial baselines using a nonlinear least-squares routine over the range of 1200–1350 cm^{-1}. Spectra of the films were acquired at least 30 min after closing the leak valve to eliminate background absorption during the remainder of the experiment, and quantified by integration of the total O–D signal located near 2600 cm^{-1}. Under these conditions, background adsorption was observed to be negligible over a period of hours. Confirmation of ASW growth is straightforward with RAIRS—the peak shapes are easily distinguished from crystalline films (CI) by inspection.[2,36,37]

CF$_4$ beams were produced by expanding a mixture of $\approx$1% CF$_4$ seeded in H$_2$ at a stagnation pressure of 300 psi through a 15 μm Pt pinhole. The nozzle could be resistively heated from room temperature to 700 K and the temperature was controlled by a Eurotherm 818 controller to maintain stable nozzle temperatures, and correspondingly stable CF$_4$ translational energies. The translational energy of CF$_4$ used in the RAIRS experiments ranged from 2.3 eV to 5.4 eV with a width ($\Delta E/E$) of 16% as measured by TOF techniques uti-

lizing a mechanical chopper and an in-line mass spectrometer. In order to quantify the flux of each CF$_4$ mixture, the signal at m/z = 69 of the chamber's background gas analyzer was calibrated to that of a pure CF$_4$ beam. The flux of the pure beam was calculated from the pressure rise in the chamber as measured by an ionization gauge, taking into account the difference in electron ionization cross section of CF$_4$ relative to N$_2$.[38,39] Unless otherwise noted, the CF$_4$ impinged upon the ice surface at normal incidence.

III. RESULTS AND DISCUSSION

A. Thermal desorption

For the thermal desorption experiments, both CF$_4$ and Xe could be detected. Illustrative results are shown in Figure 1 for both ASW and CI for 30 min exposures with nearly the same fluxes of either CF$_4$ or Xe. Figure 1(a) also shows the TPD results for ASW and CI D$_2$O. The ASW shows an initially faster desorption than CI, before the ASW converts to CI.[27] For the Xe, Figures 1(a) and 1(b), the TPD spectra show two distinct features for embedding into ASW. The low temperature peak occurs before there is any measurable D$_2$O desorption. The higher temperature feature occurs where the D$_2$O desorption becomes appreciable. Since the exposures are nearly identical, it is clear that the embedding rate is directly related to the incident energy. For the CI, there is only one feature,
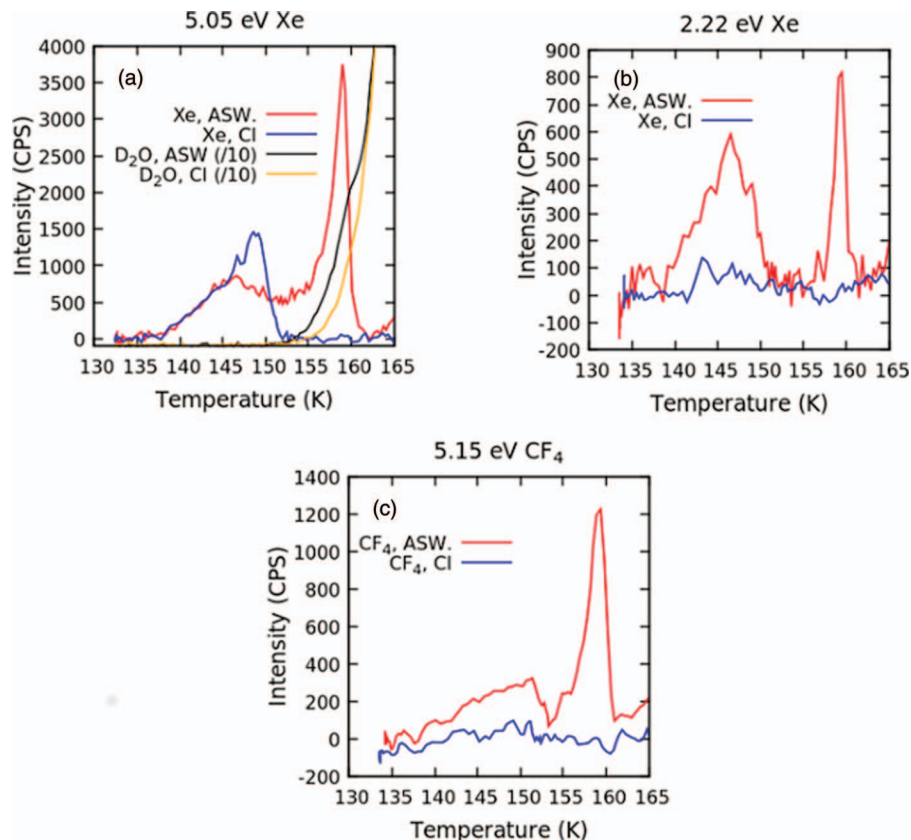

FIG. 1. Example TPD spectra for CF$_4$ and Xe. For all of the TPD spectra, the ramp rate was 10 K/min. The exposures were all done at $T_S = 120$ K, $\theta = 0°$, and for 30 min. The fluxes were nearly identical: 1.0×10^{14} Xe atoms cm^{-2} s^{-1} for (a), 1.1×10^{14} Xe atoms cm^{-2} s^{-1} for (b), and 1.1×10^{14} CF$_4$ molecules cm^{-2} s^{-1} for (c).
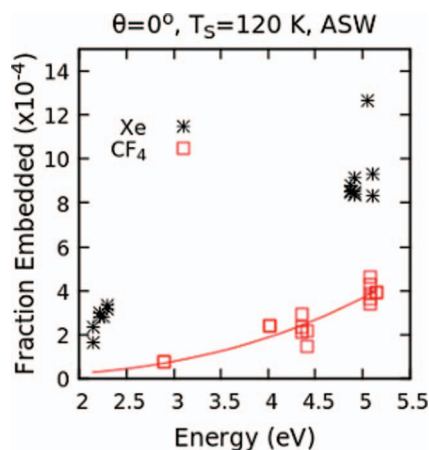
FIG. 2. Uptake rates for CF_4 and Xe on ASW as a function of incident energy for $T_S = 120$ K and $\theta = 0°$. These were determined by integrating the TPD spectra after exposure.

which occurs at a temperature below that of any measurable D_2O desorption, and only for the higher incident energy. We also dosed ASW with 0.07 eV Xe. We only saw sticking at ~ 60 K, and all of the Xe desorbed at ~ 70 K. So, none of the features in the TPD spectra shown in this paper, where exposure was done at ~ 120 K, are from *adsorbed* Xe.

   In previous papers, we also showed TPD spectra for Xe[3] and Kr.[10] The qualitative features are the same; there is a low and a high temperature feature for the ASW, with the high temperature feature occurring with the onset of appreciable D_2O desorption, and, in the case of Xe, just one feature for the CI which occurs at a temperature below which there is any significant D_2O desorption. The older Xe results show the low temperature feature extending to much higher temperatures than the spectra shown in Figures 1(a) and 1(b), but this is a result of the higher incident energy for the Xe and a much greater exposure (several thousand ML). In the previous paper on ballistic deposition,[3] we claimed that the high temperature TPD feature occurred at the ASW to CI transition. Re-examination has led us to the conclusion that the majority escapes before the transition, which is also the case for the data used for the present paper.

   Figure 1(c) shows the results for CF_4 with the nearly same incident energy as the results for Xe shown in Figure 1(a). The results have been scaled by the difference in sensitivity between CF_4 and Xe. The exposures were nearly identical, so the intensities are directly comparable. For the ASW, there are the low and high temperature features in the TPD, though the low temperature feature is less distinct. This is qualitatively similar for the results using Kr,[10] which has a similar mass. As further supported in the plot of fraction embedded vs. incident energy shown in Figure 2, it is apparent that on ASW the CF_4 embedding rate is noticeably less than the Xe embedding rate. Furthermore, while Xe embedding was observed on CI, little to no CF_4 was observed to embed in CI.

   Figure 2 shows the initial embedding rate as a function of incident energy, all at $\theta = 0°$. These are derived from the integrated TPD spectra after a long exposure. For Xe, the results in the previous paper[10] (Figure 10) showed that the amount
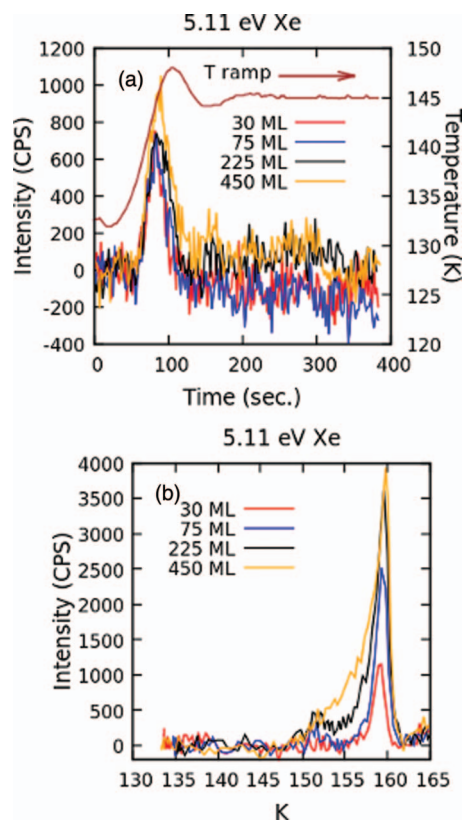

FIG. 3. Annealing at 145 K to release low temperature Xe desorption. ASW was dosed with 5.11 eV Xe at $\theta = 0°$ and $T_S = 120$ K. The Xe exposures are given in ML. (a) shows the Xe desorption as the ice is warmed to 145 K, and then held there for 300 s. The temperature profile is shown as the purple line against the right hand axis. After holding at 145 K, the ice was then cooled back to ≈ 130 K. (b) shows the Xe desorption in a TPD experiment (ramp rate = 10 K min^{-1}) of the same ice sample as it is heated above 165 K, and clearly demonstrates that the high temperature Xe desorption is not depleted by annealing at 145 K, but the low temperature desorption is eliminated. The low temperature feature also saturates much faster than the high temperature desorption feature.

absorbed rose to an asymptotic value. For the results shown in Figure 2, the total Xe exposure was less than 500 ML, which is still in an approximately linearly increasing part of the uptake curve.[10] Exposures for the CF_4 were similar, and as will be shown in Sec. III B, are also linear over these exposures. It should be noted that these are total rates; as shown in a previous paper,[2] high energy Xe can slowly sputter the ice. At 2.2 eV the rate is negligible, only 6×10^{-5} D_2O molecules per incident Xe atom. However, at 5 eV, the rate increases to 4×10^{-3} D_2O molecules per incident Xe atom. For a Xe exposure of 500 ML, ~ 1 ML of D_2O would be sputtered from the ice surface.

   As mentioned, the uptake of high energy Xe is approximately linear for low exposures. Figure 3 shows the TPD spectra for 5.11 eV Xe as a function of exposure. These TPD spectra were taken in two parts: the ice was heated to 145 K, which depleted the low temperature feature (shown in Figure 3(a)), and the sample was then cooled and the TPD repeated, *with no further Xe exposure*, to a much higher T_S so that all of the remaining Xe desorbed (shown in Figure 3(b)). The low temperature feature initially grows in very rapidly when exposure is begun, and then much slower after longer
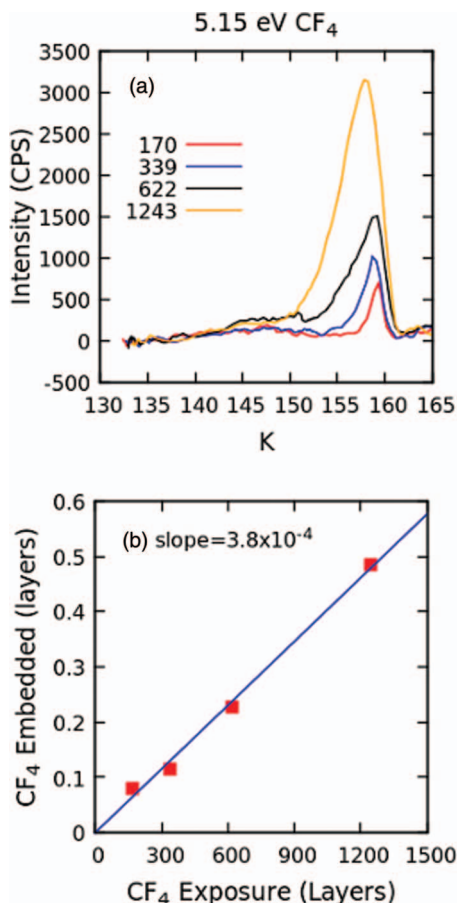
FIG. 4. Panel (a) shows the TPD spectra for 5.15 eV CF_4 as a function of exposure in ML at $\theta = 0°$ and $T_S = 120$ K. Panel (b) shows the uptake rate derived from the integrated intensities of the TPD spectra.

FIG. 5. Capping experiments for Xe. ASW at $T_S = 120$ K was exposed to 4.9 eV Xe with a flux of 1.6×10^{14} atoms cm^{-2} s^{-1} for 30 min at $\theta = 0°$. It was then beam dosed with the indicated amount of D_2O. The TPD spectra were taken in two parts, first to 145 K (a) (the temperature profile is also shown), and then cooled before another TPD spectra was taken to a temperature well past D_2O desorption (b).

exposures. The higher temperature peak fills in at an approximately linear rate for these exposures. For the CF_4, the embedding rate is quite linear to high exposures. Figure 4 shows the comparison of TPD spectra for different exposures. The CF_4 has a very intense IR signal, and the uptake will be discussed more thoroughly in Sec. III B.

Both CF_4 and Xe show the low and high temperature features in the TPD for ASW. CI shows a similar low temperature desorption feature when exposed to high energy Xe. In previous papers,[10,24] we examined the scattering of rare gases (Xe and Kr) from both ASW and CI. These papers included realistic simulations, using as a model the {0001} surface of hexagonal ice. This model would most closely resemble the crystalline CI, so it is tempting to assign the low temperature desorption feature to processes determined by the simulations. Though ASW is much more disordered, ASW has a large degree of a similar short range order.[40] Some of the conclusions from the simulations were that at high energies and normal incidence, Xe could penetrate two or three water layers below the ice surface and become at least transiently trapped, exchanging most of the incident kinetic energy with the ice lattice. As the incident energy decreases, so does the average depth of penetration.

Much of the low temperature desorption occurs between 140 and 150 K. In this temperature range, we saw no measurable D_2O desorption. Using the Arrhenius parameters from
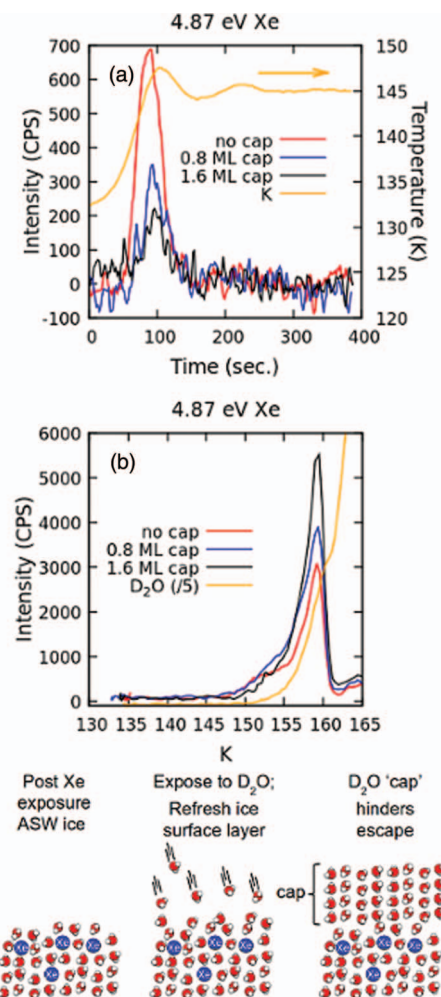
Smith *et al.*,[28] the expected desorption rate for ASW is 1×10^{-3} ML s^{-1} at 140 K, and only 3×10^{-2} ML s^{-1} at 150 K. For CI, the desorption rates are even lower: 4×10^{-4} ML s^{-1} at 140 K and 1×10^{-2} ML s^{-1} at 150 K. The absorbed gas must be percolating up from the selvedge. By stopping the TPD at an intermediate temperature, it is possible to deplete the species that leads to the low temperature peak, without any appreciable change in the intensity of the higher temperature feature. Examples are shown for Xe in Figure 5 and CF_4 in Figure 6. Both of these are two part spectra like those of Figure 3. As shown in Figure 1(c), the low temperature feature for CF_4 extends to higher temperatures than is the case for Xe. This is also shown in a comparison of Figures 5 and 6; the CF_4 dosed surface must be heated to a higher temperature to completely desorb the CF_4 from the absorption sites that lead to the low temperature TPD feature.

Also shown in Figure 5 are the results for experiments where the surface of ice, which already had embedded Xe, was exposed to a small amount of D_2O at $T_S = 120$ K before desorption. This additional water will "cap" the ice surface
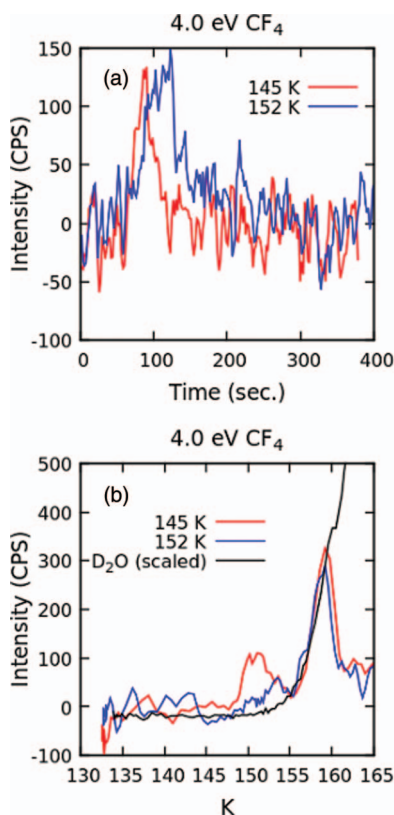
FIG. 6. Two part TPD spectra for CF$_4$. ASW at T$_S$ = 120 K was exposed to 4.0 eV CF$_4$ with a flux of 1.2 × 10^{14} CF$_4$ molecules cm^{-2} s^{-1} for 30 min at $\theta = 0°$. The TPD spectra were taken in two parts, first to 145 K or 152 K (a), and then cooled before another TPD spectra was taken to a temperature well past D$_2$O desorption (b).

embedded with Xe, further burying the implanted Xe, hindering its escape. Less than 2 ML of D$_2$O almost completely suppresses the low temperature desorption and most of the Xe desorbs at the high temperature. It should be noted that the time at which the peak desorption occurs does not change within our experimental error. Presumably, these observations indicate the Xe in this desorption channel exists just below the surface layer, and the top layer is perturbed enough that the molecules can rearrange at a relatively low temperature, and allow the Xe atoms to escape. Capping introduces an unperturbed overlayer, and the Xe stays trapped until the D$_2$O starts desorbing.

For the ASW, there is also a desorption peak that occurs concurrently with the desorption of appreciable amounts of D$_2$O. It is important to point out that this is not the "molecular volcano" that occurs at the ASW to CI transition,[41] but is trapped gas being released as the D$_2$O overlayers desorb. The peak in the CF$_4$ and Xe desorption occur between 159 and 160 K. By integrating the mass spectrometer signal at m/e = 20 of the D$_2$O TPD up to these temperatures, the amount of D$_2$O desorbed is between 2.5 and 4 ML. We do not know what the mobility of the Xe or CF$_4$ is as the temperature increases and the ice softens, but this result would suggest that the trapped Xe or CF$_4$ that leads to this desorption channel is only the equivalent of a few D$_2$O layers below the surface. This observation also qualitatively agrees with the simulations; some Xe can penetrate a few layers below the surface.
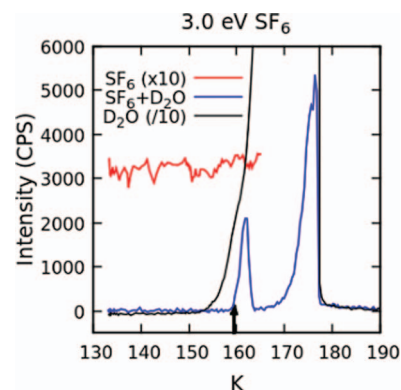

FIG. 7. ASW was exposed to 3.0 eV SF$_6$ at T$_S$ = 120 K and $\theta = 0°$ for 30 min. We did not explicitly measure the flux, but they should be similar to those for Xe and CF$_4$. The red line labeled SF$_6$ is the TPD of an experiment where the ASW was deposited (offset from 0 counts/s for clarity) first, and then the surface was exposed to the SF$_6$ beam (consecutive dosing). The blue line labeled SF$_6$ + D$_2$O is the TPD when the Rh(111) substrate was exposed to both the D$_2$O and SF$_6$ beams at the same time (concurrent dosing). The arrow indicates the peak position of the high temperature TPD feature in the embedding experiments with CF$_4$ and Xe.

To summarize, we are assigning the low temperature TPD feature to gas absorbed just below the surface layer, and the higher temperature feature largely due to gas absorbed a few layers down. The simulations[24] showed that between 20% and 80% of the Xe could remain trapped inside the ice until the calculation was stopped at 6 ps. Our experiments last for many minutes, so it may be possible for the D$_2$O molecules to rearrange over a longer time scale and eventually eject the absorbed gas. Just such a process was seen for high energy Xe that penetrated an ordered 1-decanethiol monolayer.[42]

We do not know the nature of the different absorption sites which allow for the ASW to have absorption at apparently larger depths than CI, even at the highest translational energy of 5.2 eV with $\theta = 0°$. One consideration in collisions is the momentum of the projectile. When the momentum of the Xe is lowered, it no longer absorbs into the CI. This is shown in Figure 1; 2.2 eV Xe has a lower momentum than 5.2 eV CF$_4$. To investigate further, we tried the experiments with SF$_6$, which is 1.11 times heavier than Xe. We prepared the SF$_6$ in H$_2$, and found that it was stable to at least a 473 K nozzle temperature. At 673 K, it decomposed in the hot stainless steel nozzle assembly. Results are shown in Figure 7 for an incident energy of 3 eV incident at $\theta = 0°$ on ASW. There is no detectable desorbing SF$_6$ for exposures as great as those used for Xe and CF$_4$, at 2 or 3 eV on either ASW or CI, even at $\theta = 0°$. At these energies, both Xe and CF$_4$ will at least absorb into ASW. One difference among these three molecules is their relative size. For a comparison, we estimated the sizes from the van der Waals gas constants.[43] The radii are 2.73 Å for Xe, 2.93 Å for CF$_4$, and 3.27 Å for SF$_6$. This suggests that the size has some effect. Possibly, the molecule interacts with a few more water molecules on the surface that prevents it from forming a path into the selvedge. Another possibility is that it does penetrate, but it perturbs the ice enough that it is rapidly expelled from the selvedge.

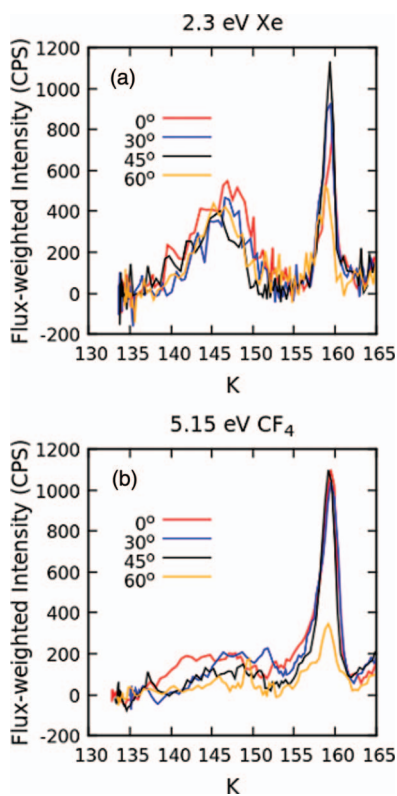Figure 7 also shows the results when the SF$_6$ and D$_2$O are dosed simultaneously. The D$_2$O flux was 0.45 ML s^{-1},

FIG. 8. (a) and (b) TPD spectra for exposures at different θ. All are for ASW at $T_S = 120$ K. Results have been corrected for flux, which changes by $1/\cos(\theta)$, either by adjusting the dosing time or the intensity.
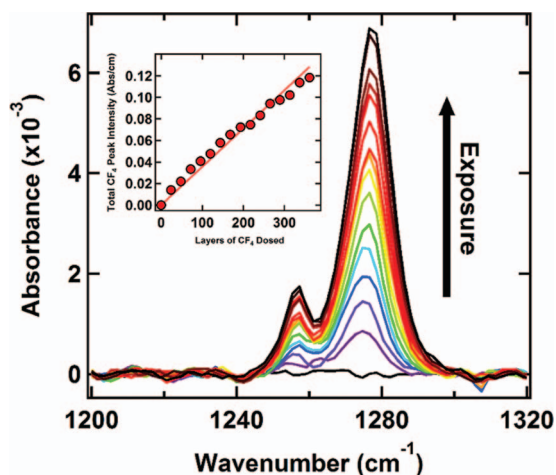

FIG. 9. Energetic ballistic deposition of 5.3 eV CF_4 into ASW ice is characterized by the appearance of RAIRS peaks at 1276 and 1257 cm^{-1}, the intensity of which increases linearly with respect to the total amount of CF_4 dosed onto the surface at normal incidence. Inset graph details the linear dependence, the slope of which is taken as the initial rate of embedding into 60 layers of ice.

$\theta = 45°$, and $T_S = 120$ K, where the deposited D_2O forms ASW. The SF_6 is entrapped throughout the ice, some comes out as a "molecular volcano," with one narrow desorption peak at the position of the ASW to CI transition, where the near surface molecules can escape as cracks form in the ice.[41] The more deeply absorbed SF_6 then desorbs in concert with the D_2O desorption. We show this experiment to demonstrate that we can easily detect SF_6, and also show that there is a fundamental difference between our ballistic absorption experiments, and the entrapping of gases with a large concurrent water flux.

The simulations[24] predict that the Xe penetration greatly decreases at more glancing incident angles. Figure 8 shows some results for 2.3 eV Xe and 5.2 eV CF_4 as a function of θ. The results show no major change until θ becomes quite glancing. It is worth noting that the surfaces showed no specular scattering of an 18 meV He beam, a strong indication that the surface is not flat on the molecular scale, so the local normal of the surface may be ill defined.

B. RAIRS

CF_4 uptake by ASW D_2O ice was confirmed with the reproducible appearance of peaks at 1276 and 1257 cm^{-1} upon exposure of the ice to the CF_4 beam at a variety of incident translational energies. An example of embedding with an incident CF_4 translational energy of 5.3 eV is detailed in Figure 9. Observed peak locations correspond to the Fermi resonance of the ν_3 asymmetric stretch and the first overtone

of the ν_4 deformation. The peaks are red-shifted from the gas phase values (1283 and 1261 cm^{-1}, respectively),[44,45] a phenomenon often observed for species physically adsorbed to or bound within an inert matrix.[46] These values are not red-shifted towards values observed for condensed phases with significant CF_4–CF_4 intermolecular interaction,[46,47] and thus the CF_4 molecules are sparsely dispersed among the D_2O molecules in the ice film. We did not look for any decomposition. The C–F bond energy is 5.7 eV,[48] as high or higher than the average translational energies we investigated. Also, from our scattering experiments,[24] we know that the ice is good at adsorbing the translational energy of the incoming projectile. Thus, it is unlikely the CF_4 decomposed.

Given that sticking is observed to be negligible at this temperature, we infer that the mechanism behind CF_4 uptake is that of energetic ballistic deposition, akin to what has been previously observed for Kr and Xe in H_2O and D_2O ices.[3,10] However, there are several instances of deviation from embedding of rare gases. From Figure 10, for example, CF_4 embedding at 3.8 eV was not observed to saturate after more than 10 000 layers of CF_4 were dosed. This distinctly contrasts the case of rare gas embedding, where saturation occurred after dosing only 4000 layers of either Kr or Xe embedding into ASW and CI crystalline ices.[10] In the same study, it was observed that ∼3 eV Kr and Xe deposition saturated near a total uptake of ∼0.5 layers. For purposes of comparison to the Xe data, we have related the total CF_4 flux to a measure of "layers of CF_4" by approximating the packing density of a CF_4 monolayer as being comparable to that of Xe given its similar size. Given the comparable size of CF_4 to Kr and Xe, as well as the similar energy used in the saturation experiment detailed in Figure 10, we make the assumption that CF_4 saturates at this same level; the CF_4 molecules' access below the second ice layer is not probable. Applying a simple Langmuir adsorption treatment to the data (see inset of Figure 10), the IR intensity can be expected to saturate at 0.18 ± 0.01 for 3.8 eV CF_4 under current instrumental conditions, and we take this intensity
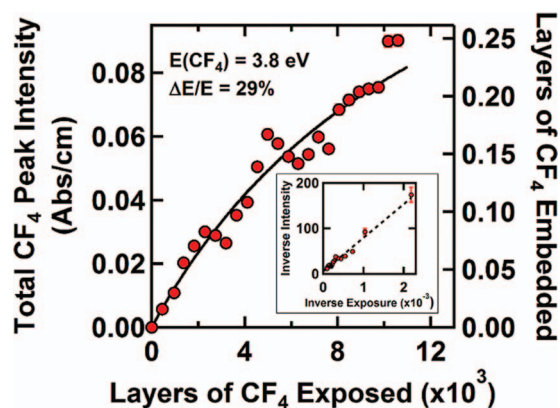
FIG. 10. Total CF$_4$ in the ice is not observed to saturate after exposure to more than 10 000 layers of CF$_4$ as measured by RAIRS, in contrast to the trend observed with rare-gas-embedding which saturates by 4000 layers of exposure in both ASW and CI ice films. The curved solid line is the Langmuir isotherm fit to the data as determined by a linear least-squares fit shown in the figure's inset. The saturation experiments were performed with a 30 μm nozzle at 120 psi (gauge) in order to maximize CF$_4$ flux, which in turn yielded a larger incident CF$_4$ energy distribution of 29%. Error bars (where visible) indicate one standard deviation with respect to the integration of peaks fit to the IR data.

to be that of a half-monolayer, yielding a conversion factor for the IR data of 2.8 ± 0.2 layers per integrated absorbance unit.

The initial rates for CF$_4$ embedding are observed to be linear in all cases, with observable embedding occurring above a translational energy threshold near ∼3.0 eV, as determined by RAIRS. As the CF$_4$ energy is increased from this critical embedding energy, the embedding rate is observed to monotonically increase for energies up to at least 5.7 eV, as detailed in Figure 11. It is important to note that the measured rates represent that of an ensemble of CF$_4$ molecules with incident energy distributions centered about the quoted values, which must be deconvoluted. To extract the true energy dependence of the embedding rate from the data, a polynomial nonlinear least-squares fit to the data, $f(E)$, was employed as an ansatz for the actual rate dependence and deconvoluted from the incident energy distribution, $P(E)$, to give the mea-
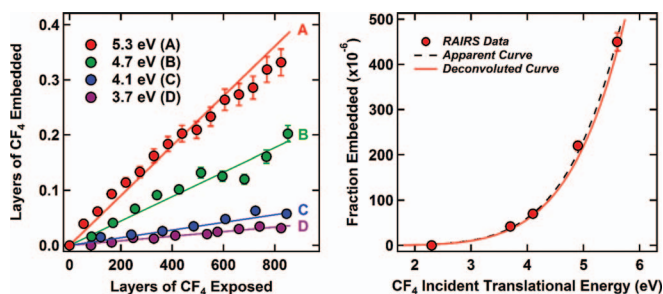
sured dependence, $F(E)$, as plotted in Figure 11,

$$F(E) = \int f(E) \cdot P(E) \cdot dE. \qquad (1)$$

In this case, deconvolution yields a curve nearly identical to the experimental curve, likely due to consecutive data points being spaced apart by an amount similar to the typical energy distribution width. Additionally, data derived from the independent TPD experiments are qualitatively consistent with the curve determined by RAIRS, lending credence to the fidelity of the results overall.

C. Comparison of the results

Figure 12(a) shows a summary of results for the rare gases Kr and Xe from TPD experiments, as previously reported.[10] These data show that the initial uptake rate has the general trends already discussed; the rate of embedding increases with energy, and for the same incident energy, the higher mass has the higher rate. In addition, these experiments show that as the amount of absorbed atoms increases, the rate decreases and seems to be reaching a plateau at ∼1 ML of absorbed gas. The densities of ASW and CI are rather similar, so it is reasonable that the number density of water molecules per unit volume are similar for the two morphologies; in that case, with the embedded gas evenly distributed throughout the
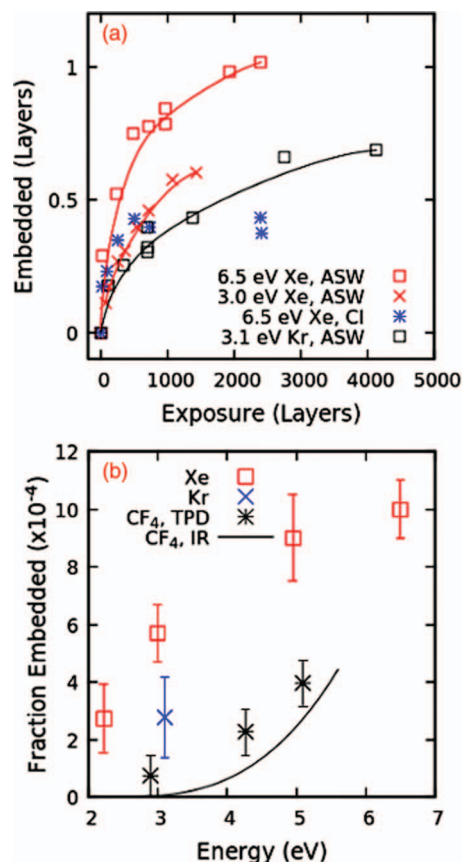

FIG. 11. Representative initial embedding fractions of CF$_4$ into 60 layers of ASW D$_2$O ice as measured by RAIRS (left). In all cases, uptake was observed to be linear, with higher rates observed for higher-energy CF$_4$. Error bars (where visible) take into account both the error in the conversion factor and one standard deviation with respect to the integration of peaks fit to the IR data. The energy dependence of embedding rate (right): dashed line indicates the polynomial fit to the apparent dependence derived from experimental data (solid circles), solid line indicates deconvoluted fit (see text). Embedding of CF$_4$ is only observed to occur above a threshold near ∼3.0 eV. Error bars (where visible) represent 95% confidence intervals for the linear fits.

FIG. 12. Figure 12(a) shows the layers of embedded rare gas as a function of exposure (from Gibson *et al.*[10]). Figure 12(b) is the initial uptake rate as a function of energy. The line for the CF$_4$ IR results is the fit shown in Figure 11.

top 4 layers, the concentration is a rather considerable 10%. Figure 12(b) shows the initial uptake rate as a function of incident energy. The rare gas data are taken from the results shown in Figure 2 and by straight line fits of the low exposure sections of the uptake curves in Figure 12(a). There is a slight difference between the IR and TPD results, but the agreement is very good considering the different experimental methods and the approximations that went into estimating absolute values of the flux and coverage. What is clear is the large difference in the initial embedding rate for Xe and CF_4.

IV. CONCLUSIONS

Our previous papers showed that high energy rare gases could be embedded in ice.[3,10,24] The rate of embedding and the final amount embedded appears to be dependent upon both the energy and mass of the projectile, though always rather small. The rate decreases as gas is embedded, with the asymptotic value increasing for greater energy and mass, possibly because the atoms can penetrate further into the bulk. The TPD results for the embedding of Xe in CI vary from those for ASW, as most of the embedded Xe escapes at a temperature below any appreciable water desorption.

This paper expands on those observations, using both TPD and RAIRS experiments. We looked at three inert projectiles: Xe, CF_4, and SF_6. Using TPD experiments, we showed that for Xe and CF_4, the embedded gas that escapes at the lowest temperatures appears to be absorbed just below the surface. The remaining embedded gas escapes as the water desorbs, with the majority coming off by the time the equivalent water desorption is 2.5–4 layers of hexagonal ice. This is in agreement with scattering calculations for Xe from the surface of hexagonal ice.[24] The embedding rate of CF_4 (2/3 the mass of Xe) in ASW is always much lower than Xe at the same incident energy. CF_4 does not embed in CI at even the highest observed energies (∼5.7 eV).

We explored the embedding of SF_6 into ASW by exposing the ice to a SF_6 beam with a translational kinetic energy of 3 eV. This is slightly more massive than Xe (146 g mol^{-1} vs. 132 g mol^{-1}), but there was no indication of any embedding into ASW, even though this is approximately the lowest energy for detecting CF_4 embedding, and Xe definitely embeds. One difference between SF_6 and the other gases is its van der Waals radius; it is significantly larger. Possibly, the larger size perturbs the surrounding water molecules enough that it is pushed out by rearranging molecules, as was observed for high energy Xe penetrating below the surface of a self-assembled monolayer.[42]

The results discussed in this paper have expanded significantly on the previous experimental and theoretical work. We know from calculations[10,24] for high energy Xe impinging on hexagonal ice that the Xe can penetrate several layers below the surface, and remain trapped for significant lengths of time. The depth of deepest penetration decreases with decreasing incident energy.[24] This could help explain why the final amount of embedded Xe is less for 3.0 eV than 6.5 eV.; the higher energy Xe penetrates deeper into the selvedge. A similarly sized but less massive inert projectile CF_4, also embedded, but at a much slower rate. A heavier, but also larger projectile, SF_6, did not embed. These results offer tantalizing clues as to the nature of the embedding of gases into ice. There is also the difference between CI and ASW results, which indicate fundamental differences between the near surface structures of these two forms of ice.

These results show that energetic ballistic embedding in ice is a general phenomenon for both atomic and molecular species, and represents a significant new channel by which incident species can be trapped under conditions where they would otherwise not be bound stably as surface adsorbates. These findings have implications for many fields including environmental science, trace gas collection and release, and the chemical composition of astrophysical icy bodies in space.

[1] A. Bar-Nun, G. Notesco, and T. Owen, Icarus **190**, 655 (2007).

[2] D. R. Killelea, K. D. Gibson, H. Yuan, J. S. Becker, and S. J. Sibener, J. Chem. Phys. **136**, 144705 (2012).

[3] K. D. Gibson, D. R. Killelea, J. S. Becker, H. Yuan, and S. J. Sibener, Chem. Phys. Lett. **531**, 18 (2012).

[4] G. Strazzulla, G. Leto, O. Gomis, and M. A. Satorre, Icarus **164**, 163 (2003).

[5] O. Gomis, M. A. Satorre, G. Strazzulla, and G. Leto, Planet. Space Sci. **52**, 371 (2004).

[6] G. Strazzulla, G. A. Baratta, G. Leto, and O. Gomis, Icarus **192**, 623 (2007).

[7] G. Strazzulla, Nucl. Instrum. Methods Phys. Res. B **269**, 842 (2011).

[8] R. Yokochi, U. Marboeuf, E. Quirico, and B. Schmitt, Icarus **218**, 760 (2012).

[9] F. W. Karasek, R. E. Clement, and J. A. Sweetman, Anal. Chem. **53**, 1050A (1981).

[10] K. D. Gibson, D. R. Killelea, H. Yuan, J. S. Becker, S. Pratihar, P. Manikandan, S. C. Kohale, W. L. Hase, and S. J. Sibener, J. Phys. Chem. C **116**, 14264 (2012).

[11] M. F. A'Hearn, L. M. Feaga, H. U. Keller, H. Kawakita, D. L. Hampton, J. Kissel, K. P. Klaasen, L. A. McFadden, K. J. Meech, P. H. Schultz, J. M. Sunshine, P. C. Thomas, J. Veverka, D. K. Yeomans, S. Besse, D. Bodewits, T. L. Farnham, O. Groussin, M. S. Kelley, C. M. Lisse, F. Merlin, S. Protopapa, and D. D. Wellnitz, Astrophys. J. **758**(29), 1 (2012).

[12] G. Notesco, A. Bar-Nun, and T. Owen, Icarus **162**, 183 (2003).

[13] T. Owen and A. Bar-Nun, Icarus **116**, 215 (1995).

[14] D. J. Burke and W. A. Brown, Phys. Chem. Chem. Phys. **12**, 5947 (2010).

[15] P. Ehrenfreund and S. B. Charnley, Annu. Rev. Astron. Astrophys. **38**, 427 (2000).

[16] P. G. Brewer, F. M. Orr, G. Friederich, K. A. Kvenvolden, and D. L. Orange, Energy Fuels **12**, 183 (1998).

[17] C. Krauss and S. Saulny, N. Y. Times (11 May 2010), p. A12.

[18] M. K. McNutt, R. Camilli, T. J. Crone, G. D. Guthrie, P. A. Hsieh, T. B. Ryerson, O. Savas, and F. Shaffer, Proc. Natl. Acad. Sci. U.S.A. **109**, 20260 (2012).

[19] D. J. Wuebbles and K. Hayhoe, Earth-Sci. Rev. **57**, 177 (2002).

[20] P. Bousquet, P. Ciais, J. B. Miller, E. J. Dlugokencky, D. A. Hauglustaine, C. Prigent, G. R. Van der Werf, P. Peylin, E. G. Brunke, C. Carouge, R. L. Langenfelds, J. Lathiere, F. Papa, M. Ramonet, M. Schmidt, L. P. Steele, S. C. Tyler, and J. White, Nature (London) **443**, 439 (2006).

[21] G. J. Macdonald, Clim. Change **16**, 247 (1990).

[22]O. B. Toon, R. P. Turco, J. Jordan, J. Goodman, and G. Ferry, J. Geophys. Res. **94**, 11359, doi:10.1029/JD094iD09p11359 (1989).

[23]R. P. Turco, O. B. Toon, and P. Hamill, J. Geophys. Res., [Atmos.] **94**, 16493, doi:10.1029/JD094iD14p16493 (1989).

[24]S. Pratihar, S. C. Kohale, L. Yang, P. Manikandan, K. D. Gibson, D. R. Killelea, H. Yuan, S. J. Sibener, and W. L. Hase, J. Phys. Chem. C **117**, 2183 (2013).

[25]A. P. Graham and J. P. Toennies, J. Chem. Phys. **118**, 2879 (2003).

[26]R. S. Smith, C. Huang, E. K. L. Wong, and B. D. Kay, Surf. Sci. **367**, L13 (1996).

[27]R. J. Speedy, P. G. Debenedetti, R. S. Smith, C. Huang, and B. D. Kay, J. Chem. Phys. **105**, 240 (1996).

[28]R. S. Smith, J. Matthiesen, J. Knox, and B. D. Kay, J. Phys. Chem. A **115**, 5908 (2011).

[29]K. D. Gibson, M. Viste, and S. J. Sibener, J. Chem. Phys. **112**, 9582 (2000).

[30]D. E. Brown, S. M. George, C. Huang, E. K. L. Wong, K. B. Rider, R. S. Smith, and B. D. Kay, J. Phys. Chem. **100**, 4988 (1996).

[31]K. P. Stevenson, G. A. Kimmel, Z. Dohnálek, R. S. Smith, and B. D. Kay, Science **283**, 1505 (1999).

[32]G. A. Kimmel, Z. Dohnálek, K. P. Stevenson, R. S. Smith, and B. D. Kay, J. Chem. Phys. **114**, 5295 (2001).

[33]U.S. Department of Commerce, N. NIST: Electron-Impact Cross Section Database   http://www.nist.gov/pml/data/ionization/index.cfm   (accessed Jun 11, 2014).

[34]F. Nakao, Vacuum **25**, 431 (1975).

[35]Y. Baskin and L. Meyer, Phys. Rev. **100**, 544 (1955).

[36]K. D. Gibson, D. R. Killelea, H. Yuan, J. S. Becker, and S. J. Sibener, J. Chem. Phys. **134**, 034703 (2011).

[37]R. Smith, T. Zubkov, and B. Kay, J. Chem. Phys. **124**, 114710 (2006).

[38]C. Ma, M. R. Bruce, and R. A. Bonham, Phys. Rev. A **44**, 2921 (1991).

[39]Y. Itikawa, J. Phys. Chem. Ref. Data **35**, 31 (2006).

[40]D. T. Bowron, J. L. Finney, A. Hallbrucker, I. Kohl, T. Loerting, E. Mayer, and A. K. Soper, J. Chem. Phys. **125**, 194502 (2006).

[41]R. A. May, R. S. Smith, and B. D. Kay, J. Chem. Phys. **138**, 104501 (2013).

[42]K. D. Gibson, N. Isa, and S. J. Sibener, J. Phys. Chem. A **110**, 1469 (2006).

[43]R. C. Reid, J. M. Prausnitz, and B. E. Poling, *The Properties of Gases and Liquids*, 4th ed. (McGraw-Hill, New York, NY, 1987).

[44]P. J. H. Woltz and A. H. Nielsen, J. Chem. Phys. **20**, 307 (1952).

[45]L. H. Jones, C. Kennedy, and S. Ekberg, J. Chem. Phys. **69**, 833 (1978).

[46]O. Byl, P. Kondratyuk, S. T. Forth, S. A. FitzGerald, L. Chen, J. K. Johnson, and J. T. Yates, J. Am. Chem. Soc. **125**, 5889 (2003).

[47]R. P. Fournier, R. Savoie, F. Bessette, and A. Cabana, J. Chem. Phys. **49**, 1159 (1968).

[48]D. F. McMillen and D. M. Golden, Annu. Rev. Phys. Chem. **33**, 493 (1982).